Cell Reports
Physical Science

CellPress
OPEN ACCESS

Article

Controlled self-assembly of a giant isohedral triakis tetrahedron

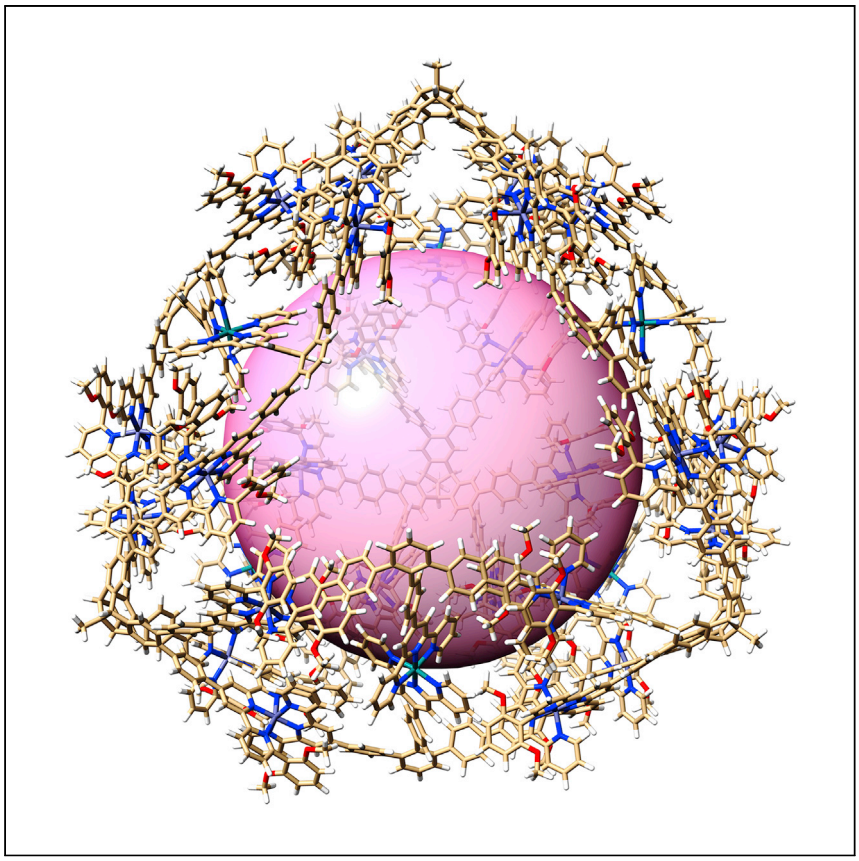

Realization of polyhedral architectures of comparable complexity to those achieved in biological assemblies is a long-running goal within materials science. Here, Jiang et al. demonstrate the formation of a unique molecular triakis tetrahedron, enriching the topological diversity of supramolecular polyhedra.

Zhilong Jiang, Jun Wang, Haixin Zhang, ..., Kun Wang, Mingzhao Chen, Pingshan Wang

kw2504@msstate.edu (K.W.)
jinyulinzhao@foxmail.com (M.C.)
chemwps@csu.edu.cn (P.W.)

Highlights

A giant tetrahedron is created through one-pot multi-component self-assembly

The triakis tetrahedron is generated from four trigonal-pyramidal cages

Controllable self-assembly improves the topological diversity of polyhedra generated

Jiang et al., Cell Reports Physical Science 4, 101293
March 15, 2023
https://doi.org/10.1016/j.xcrp.2023.101293

Cell Reports
Physical Science

CellPress
OPEN ACCESS

Article

Controlled self-assembly of a giant isohedral triakis tetrahedron

Zhilong Jiang,[1,2,3,9] Jun Wang,[1,3,9] Haixin Zhang,[5,9] Weiya Liu,[1,3] Zihao Wu,[1,2,3] He Zhao,[4] Jia-Fu Yin,[7] Bangtang Chen,[1,3] Yiming Li,[4] Panchao Yin,[7] Yi-Tsu Chan,[8] Kun Wang,[5,6,*] Mingzhao Chen,[1,2,3,*] and Pingshan Wang[1,2,3,4,10,*]

SUMMARY

Polyhedra have long appeared throughout art and design for their aesthetic topological features and, more recently, have found versatile roles in supramolecular chemistry and organized materials. Non-regular convex tetrahedra with positive augmentations of a regular tetrahedron, for example an isohedral triakis tetrahedron, have rarely been explored in synthetic chemistry. Herein, we report the synthesis of a giant triakis tetrahedron through multi-component self-assembly from four umbrella-shaped hexa-armed organic terpyridine ligands and six pre-organized cadmium-containing building blocks. Hexafunctionalized tribenzotriquinacene cavitands serve as the scaffold for the formation of the triakis tetrahedron. The convex vertices derived from rhomboid panels form four trigonal-pyramidal cages based on regular tetrahedral faces. Characterization with multiple types of nuclear magnetic resonance spectroscopy, mass spectrometry, atomic resolution microscopy, and X-ray scattering provide crucial structural information on the triakis tetrahedron. The triakis tetrahedron is applied in the photo-driven degradation of a sulfur mustard mimic. The principles developed herein enhance the possible topological diversity of supramolecular coordination polyhedra.

INTRODUCTION

The knowledge of the geometry of polyhedra has accumulated since ancient times. Polyhedral cage-like architectures, such as Platonic solids, Archimedean solids, Catalan solids, and Johnson solids, are aesthetically appealing and have received much attention from synthetic chemists.[1] Biology also shows us many polyhedral nanostructures and their assembly mechanisms,[2] such as poliovirus, which is built from 60 protein subunits that are progressively assembled into an icosahedral procapsid of the virus.[3] In the field of protein and DNA assembly, various giant-tile polyhedral architectures have been reported,[4,5] including the organization of DNA strands into larger trimeric, pentameric, or hexameric building units, which is crucial for creating polyhedral shell-like protein cages.[6] In analogy with the biological processes of rational control of paneling units, chemists have used powerful self-assembly methods to construct many analogous polyhedral cage-like molecular architectures from pre-organized building blocks.[7–10] Such structures are of interest not only because they have intrinsic aesthetic appeal but also because they help improve our understanding of self-assembly processes in biological systems. Besides, benefiting from the hollow central cavities, these synthetic structures offer potential applications in guest encapsulation,[11–14] catalysis,[15–18] separations,[19–22] and more.[23–26]

[1]Institute of Environmental Research at Greater Bay Area, Guangzhou University, Guangzhou, Guangdong 510006, China

[2]Guangzhou Key Laboratory for Clean Energy and Materials, Guangzhou University, Guangzhou, Guangdong 510006, China

[3]Key Laboratory for Water Quality and Conservation of the Pearl River Delta, Ministry of Education, Guangzhou University, Guangzhou, Guangdong 510006, China

[4]College of Chemistry and Chemical Engineering, Central South University, Changsha, Hunan 410083, China

[5]Department of Physics and Astronomy, Mississippi State University, Mississippi State, MS 39762, USA

[6]Department of Chemistry, Mississippi State University, Mississippi State, MS 39762, USA

[7]South China Advanced Institute for Soft Matter Science and Technology and State Key Laboratory of Luminescent Materials and Devices, South China University of Technology, Guangzhou 510640, China

[8]Department of Chemistry, National Taiwan University, Taipei 10617, Taiwan

[9]These authors contributed equally

[10]Lead contact

*Correspondence: kw2504@msstate.edu (K.W.), jinyulinzhao@foxmail.com (M.C.), chemwps@csu.edu.cn (P.W.)

https://doi.org/10.1016/j.xcrp.2023.101293

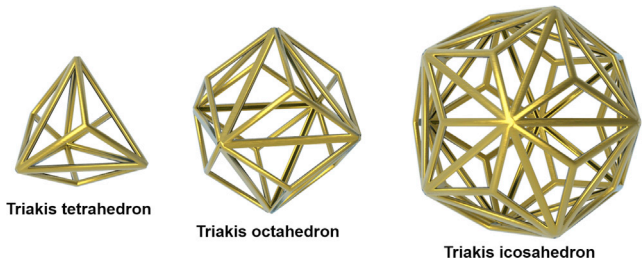

Figure 1. Schematic representation of 3D triakis geometries
Shown is a triakis tetrahedron, triakis octahedron, and triakis icosahedron.

Remarkable achievements in the synthesis of giant polyhedral cage-like architectures have been made based on hydrogen bonding or coordination chemistry through ordered fragments.[27–30] Discrete, well-defined metallo-supramolecular cages are assembled by organic ligands and metal ions with bottom-up strategies, exploiting the reversibility of coordination bonds. Most notably, in Fujita's M_nL_{2n} metallocages, in which M = Pd^{2+}, L = bend angle of dipyridine ligands, and n = 6, 12, 24, 30, and even 48, correspond to five types of polyhedra: i.e., cube,[31] cuboctahedra,[32] rhombicuboctahedra,[33] icosidodecahedra,[34] and tetravalent Goldberg polyhedra.[35] Another class of metal-organic polyhedra (MOP) that has received significant attention is carboxylic acid-based microporous cuboctahedron.[36] Besides, many groups have independently contributed to the vast library of polyhedral cages including Stang,[37] Raymond,[38] Nitschke,[7] Kim,[39] and others.[10,26,40–47] These polyhedral cages can show synthetic versatility because of their host systems and unique cavities with different sizes and shapes.[48]

Triakis solids are an uncommon family of polyhedral structures that are obtained from regular polyhedrons by adjoining to each face of the polyhedron a pyramid (based on that face) of appropriate height (Figure 1).[49] In general, a triakis tetrahedron is a non-regular dodecahedron that can be constructed as a positive augmentation of a regular tetrahedron.[50] From a synthetic-chemistry perspective, the chemical synthesis of triakis solids has rarely been realized. Although the mathematical networks are chemically feasible, obtaining "strained" frameworks with proper bond lengths and angles is extremely challenging.

Here, we report the successful realization of a giant tetrahedron that arises from four bowl-shaped hexatopic terpyridyl ligands L^3 and six complementary clip-shaped metal-organic ligands L^1. The use of complementary unit and corner directing units promotes the formation of 3D hexarhomboid architecture, which outwardly resembles the triakis tetrahedron (Figure 2). The requisite multi-topic bridging ligands were designed by employing bowl-shaped hexatopic terpyridyl ligand as the vertex and clip-shaped metal-organic ligand as the bridge. The convex vertexes derived from three adjacent rhomboid panels form four trigonal-pyramidal cages based on regular tetrahedral faces (Figure S1). Molecular triakis tetrahedron S^2 was formed in near-quantitative yield by one-pot multi-component self-assembly of L^1 with L^3 in the presence of metal ions. Differing from previously reported work, the use of rigid hexatopic organic ligand as the corner directing unit and stable metallo-organic ligand (MOL) as the acceptor promotes the efficient formation of the desired isohedral triakis tetrahedron. The diameter of the obtained triakis tetrahedron reaches 5.3 nm, which is greater than most metal (metalloid) clusters and polyoxometallates. ^{1}H nuclear magnetic resonance (NMR), 2D diffusion-ordered spectroscopy (DOSY), electrospray ionization mass spectrometry (ESI-MS), and ESI-traveling wave ion

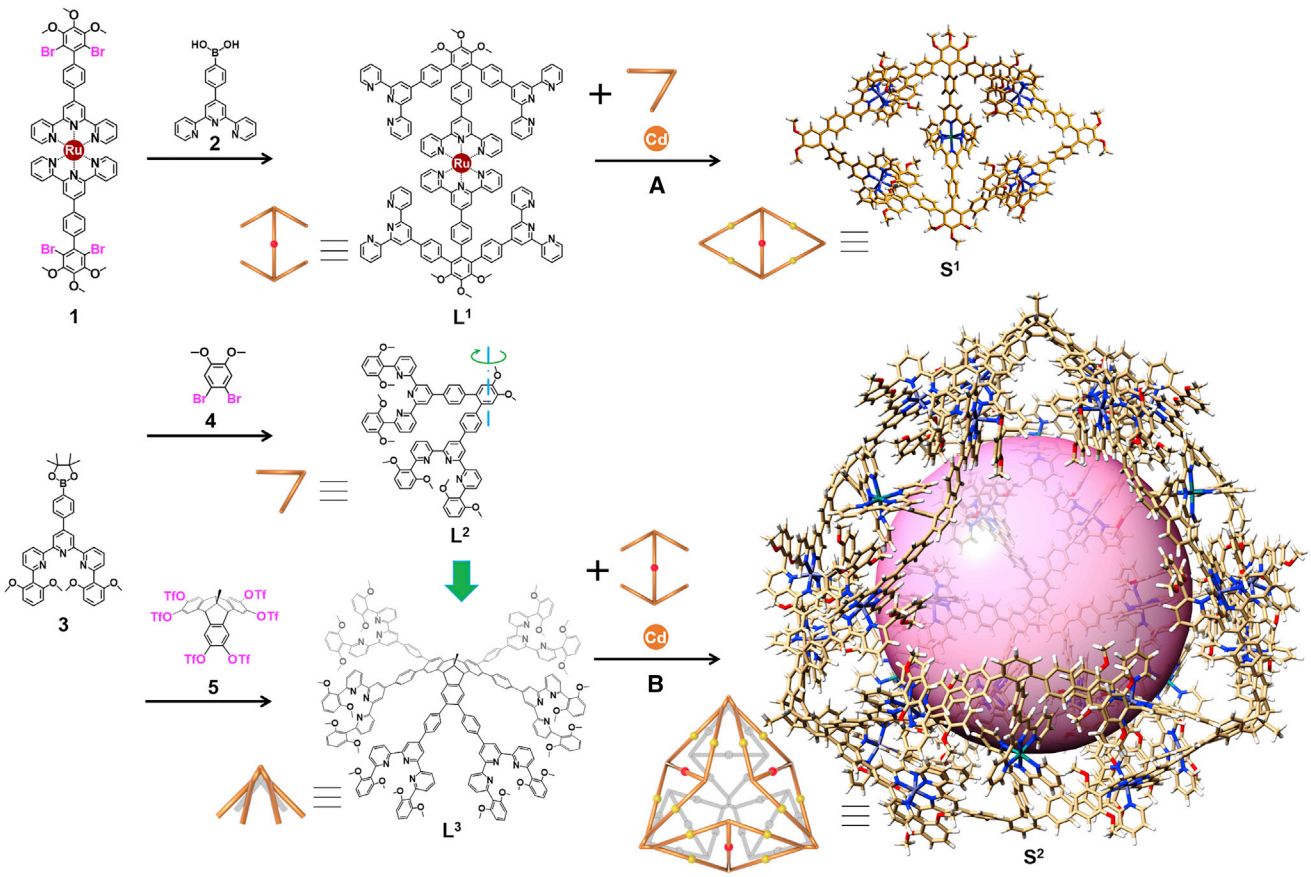

Figure 2. The synthetic strategy of ligands and their assemblies

(A) Multi-component self-assembly of rhombic supermolecule S^1.

(B) Multi-component self-assembly of triakis tetrahedra supramolecule S^2.

mobility (TWIM)-MS were employed to support the formation of supramolecular coordination complexes. Furthermore, transmission electron microscope (TEM), scanning tunneling microscope (STM), atomic force microscope (AFM), and small-angle X-ray scattering (SAXS) measurements were performed to provide crucial structural information.

RESULTS AND DISCUSSION

Design and synthesis of ligands and their assemblies

In order to obtain stable 3D giant structures through one-step heteroleptic self-assembly without troublesome separation processes, the structure of skeletons in the vertex ligands with multi-valency and complementary complexation is of utmost importance.[51] Accordingly, MOL L^1 with four free terpyridine coordinated sites was picked to promote the complementary rhombic shape-defining self-assembly; by the introduction of stable tpy-Ru^{2+}-tpy connectivity, the stability of the final structure was enhanced to ensure the feasibility of quantitative assembly and eliminate possible by-products. The detailed synthetic routes and steps for the MOL L^1 were presented in ESI. The ^{1}H NMR spectrum of MOL L^1 shows a series of signal peaks; in the aromatic region, two single peaks at 8.94 and 8.72 ppm with 1:2 integral proportion attributed to coordinated and uncoordinated Tpy-$H^{3',5'}$ protons were observed, and two singlets at 4.16 and 3.77 ppm with a 1:2 ratio were observed in the non-aromatic region (Figure 3A).

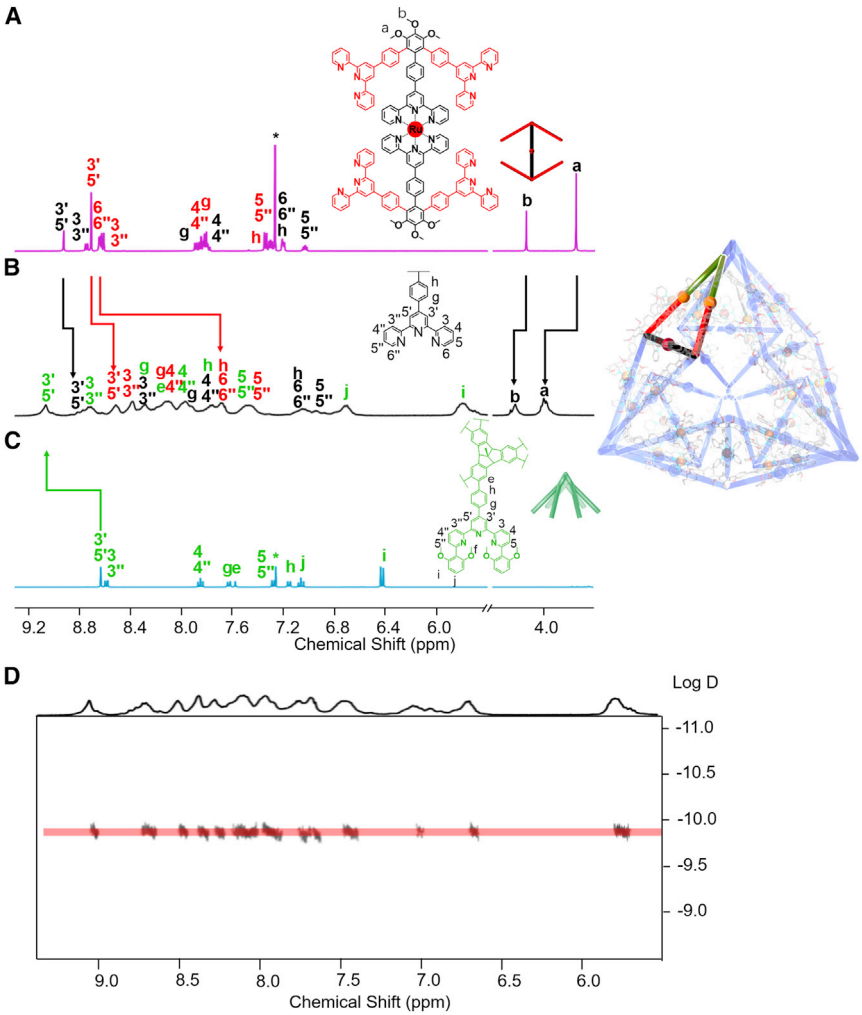

Figure 3. NMR studies of the triakis tetrahedron

(A) ^{1}H NMR spectrum (400 MHz, 298 K) of metallo-organic ligand L^1 in CD_3OD.

(B) ^{1}H NMR spectrum (400 MHz, 298 K) of triakis tetrahedron S^2 in CD_3CN.

(C) ^{1}H NMR spectrum (400 MHz, 298 K) of tribenzotriquinacene-based hexatopic terpyridine ligand L^3 in $CDCl_3$.

(D) DOSY NMR spectrum (500 MHz, 298 K) of triakis tetrahedron S^2 in CD_3CN.

For a better understanding of the 3D triakis tetrahedron structural features, the design and synthesis of 2D rhombic structure S^1 is initially involved (Scheme S1). Ditopic 60°-bent bisterpyridine L^2 was synthesized from boronic acid **3** and 1,2-dibromo-4,5-dimethoxybenzene **4**. In order to prevent the self-sorting process of L^2, the 6,6"-positions of terpyridines were decorated with 2,6-dimethoxyphenyl substituents as the bulky groups.[52] The ^{1}H NMR spectrum of ligand L^2 exhibited only one set of terpyridine characteristic signal peaks, and ESI-MS experiments further confirmed its formation. After mixing it with ligand L^1 and $Cd(NO_3)_2{\cdot}4H_2O$ in a 1:2:4 ratio in a mixed solvent of $MeCN/CHCl_3/MeOH$ (2:2:1, v/v/v), refluxed at 80°C for 12 h, a red precipitate was obtained with the addition of excess $LiNTf_2$ (dissolved in CH_3OH). The assembled product was initially identified by ^{1}H NMR and ESI-MS experiments (Figures S2 and S3).

In general, the use of multi-topic tpy ligands with non-planar directionality is vital toward the direct self-assembly of a 3D supramolecular architecture. Since rhombic

structure S^1 is planar and rigid, a non-planar core that can provide multi-topic bridges is necessary for the formation of 3D triakis tetrahedron S^2. A ligand based on bowl-shaped tribenzotriquinacene perfectly meets this requirement. Multi-topic bridging ligand L^3 was designed by employing bowl-shaped tribenzotriquinacene as the corner directing unit vertex. Ligand L^3 with perfect C_3 symmetry contains three 60°-bent non-planar bisterpyridines and shows good dendritic distribution. The ^{1}H NMR spectrum of ligands L^3 exhibited one set of tpy-$H^{3',5'}$ protons, indicating it possesses a high degree of structural symmetry (Figure 3C).

Characterization of triakis tetrahedron S^2

Given the good kinetic reversibility and self-correction of $[Cd(tpy)_2]^{2+}$, Cd^{2+} ions were chosen for the synthesis of the giant triakis tetrahedron S^2. After one-pot multi-component self-assembly of L^1 and L^3 with a 2:3 ratio under the existence of enough Cd^{2+} ions, a red solid product S^2 was generated in nearly quantitative yield (97%). The ^{1}H NMR spectrum of S^2 shows broadened signal peaks (Figure 3B), suggesting the formation of giant assembly product, and all signal peaks were successfully assigned with the help of 2D COSY and 2D nuclear overhauser effect spectroscopy (NOESY) experiments (Figures S9 and S10). Two singlets at 9.06 and 8.51 ppm in a 1:1 ratio attributed to Tpy-$H^{3',5'}$ protons, and one Tpy-$H^{3',5'}$ signal peak was overlapped with other protons. In the non-aromatic region, the ^{1}H NMR spectrum exhibited three split signal peaks at 4.26–4.22, 4.02–3.98, and 2.85–2.61 ppm with an integration ratio of 1:2:8 derived from three types of methoxy units. In addition, the characteristic tpy-$H^{6,6''}$ protons of S^2 from uncoordinated terpyridines of ligand L^3 were shifted up field, apparently owing to the electron-shielding effects, indicating the successful coordination with Cd^{2+} ions. In addition, S^2 exhibits compact structural features, which are likely to limit the free rotation of the juxtaposed arms and lead to a different chemical environment for the synthesized complex. The DOSY spectrum of S^2 displayed only one narrow band at log D = −9.86 in CD_3CN at 298 K, proving the absence of other by-products in the solution (Figure 3D).

ESI-MS combined with TWIM-MS experiments were performed to further investigate the composition and purity of assembled product. As shown in Figure 4A, the ESI-MS spectrum of S^2 displayed a series of signal peaks with successive charge states from 37+ to 18+ at *m/z*: 1,024.76; 1,061.02; 1,099.39; 1,139.83; 1,182.69; 1,228.67; 1,277.54; 1,329.12; 1,384.63; 1,444.35; 1,508.25; 1,576.98; 1,651.22; 1,731.61; 1,818.99; 1,914.59; 2,019.10; 2,133.95; 2,261.06; and 2,401.96, due to the loss of a different number of NTf_2^- anions during the ionization. The experimental *m/z* values of each charge states corresponded well with the simulate values of $[(Cd_{24}L^1{}_4L^3{}_6)\ (NTf_2^-)_{60}]$ with a molecular weight of 48,284 Da. Due to the large molecular weight of supramolecule S^2 and limited instrumentation resolution, a satisfactory isotopic pattern has not been obtained. For each charge state, minor signals can be observed behind the main peaks from incomplete anion exchange and ionization of NTf_2^- (Figure S55). Furthermore, the TWIM-MS spectrum of S^2 displayed narrow drift time distributions for the charge states from 34+ to 20+; the narrow drift time distribution indicates that no isomers or conformers exist (Figure 4B). Moreover, no signals belong to oligomers or other isomers were observed, reflecting the quantitative formation of target triakis tetrahedron S^2.

Size characterization

With a basic grasp of the molecular composition of the triakis tetrahedron S^2, a series of characterizations were performed to analyze and visualize the size and shape of individual triakis tetrahedron S^2. A TEM experiment, as a common electron

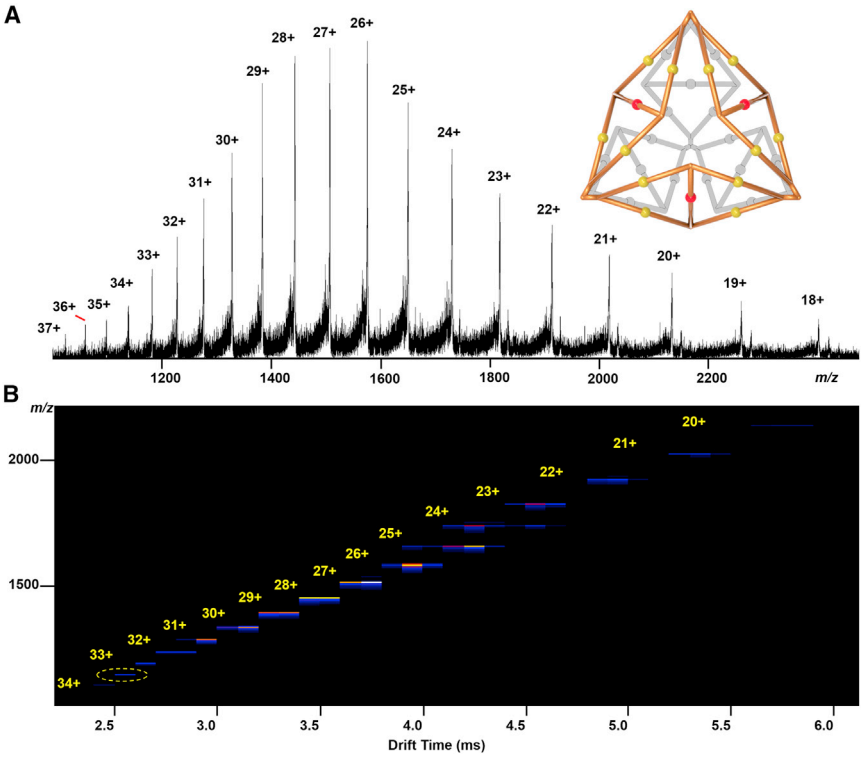

Figure 4. Mass spectrometry for characterization of the triakis tetrahedron

(A) ESI-MS spectrum of triakis tetrahedron S^2.

(B) ESI-TWIM-MS plots of triakis tetrahedron S^2.

microscope to characterize the microstructure, was used to analyze the morphology of individual triakis tetrahedron S^2. As shown in Figure 5B, the TEM image of S^2 revealed individual particles with a measured size of 5.4 $\pm$ 0.2 nm, which matched well with the dimensions of the theoretical diameter of molecular modeling (Figure 5A). The sizes were also comparable to the dynamic light scattering (DLS) experiment, which gave an average hydrodynamic size of the triakis tetrahedron S^2 of ~5.2 nm (Figure 5C).

To gain a more in-depth understanding of the molecular structure, we further carried out STM and AFM imaging for the supramolecule triakis tetrahedron S^2. For STM measurements, the supramolecule S^2 solution (~0.1 mM) was drop casted onto the surface of the freshly cleaved highly ordered pyrolytic graphite (HOPG) surface for incubation and then dried with nitrogen gas prior to STM imaging. Interestingly, the supramolecule S^2 was self-arranged into a long nanowire (Figure 5D). The zoomed-in view of the hierarchical self-arranged structure, illustrated in Figure 5E, reveals the detailed intra- and inter-molecular structural details. The less conductive region (low brightness) at the center of each individual molecule corresponds to the weaker π-π conjugation at the center of the molecule. This unique nanostructure pattern could be attributed to several possible interactions. Firstly, the π-π interaction and van der Waals interaction between the molecule and HOPG substrate facilitate the absorption of the molecule to the HOPG surface.[53,54] Secondly, inter-molecular interactions between neighboring molecules, including π-π stacking of aromatic rings, hydrogen bond formation (e.g., C–H···N), and van der Waals interactions at the interface of two adjacent molecules could assist in the formation of the

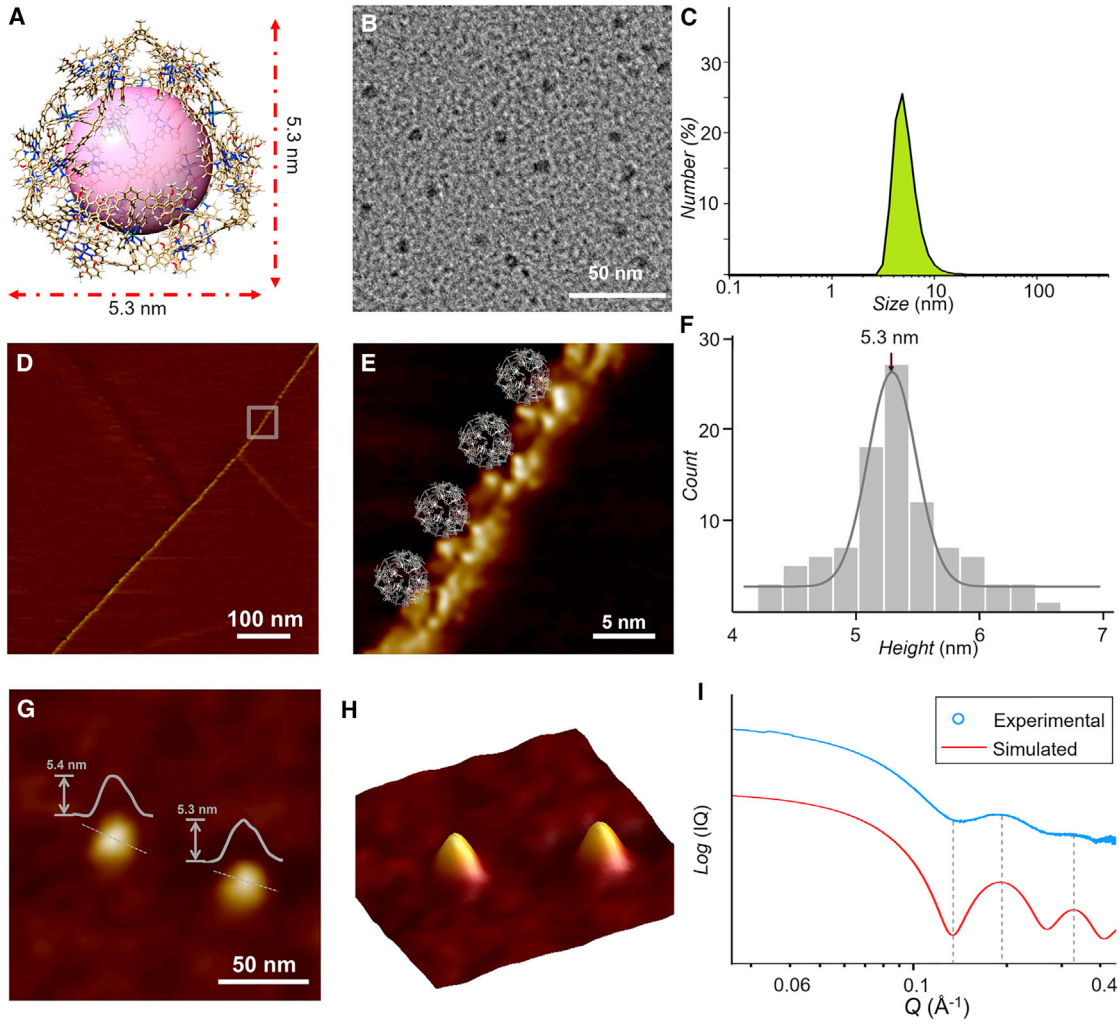

Figure 5. Molecular models and size characterization of the triakis tetrahedron

(A) Representative energy-minimized structures from molecular modeling of triakis tetrahedron S^2.
(B) TEM image of triakis tetrahedron S^2.
(C) DLS of triakis tetrahedron S^2.
(D) Triakis tetrahedron S^2 on the HOPG surface showing self-assembled nanowire-like structure. Scale bar is 100 nm.
(E) Zoom-in view of the STM image in the panel that reveals detailed structures of individual molecules. Scale bar is 5 nm.
(F) Height histogram of 98 triakis tetrahedrons S^2 on the mica surface from AFM.
(G) AFM image of triakis tetrahedron S^2. Scale bar is 50 nm.
(H) 3D AFM image of triakis tetrahedron S^2.
(I) SAXS profiles of the triakis tetrahedron S^2.

hierarchical self-assembly of the nanowire.[55] A schematic illustrating these interactions is provided in Figure S61.

While STM is suitable to visualize the molecular structure in the x-y plane, AFM is adopted to map the height profile of the 3D supramolecular structure. Therefore, given the 3D nature of the supramolecule S^2, we further performed AFM imaging of the molecule on the mica surface. As shown in Figure 5G (Figure 5H, the 3D illustration), the height of individual supramolecules is ~5.3 nm. To investigate the average molecular height, we statistically analyzed the height information of 98 discrete S^2 molecules. More AFM results are provided in Figure S60. As shown in Figure 5F, the height histogram exhibited an average molecular height of

5.29 ± 0.02 nm, which matches our molecular model, TEM, and STM results. Moreover, comparing the STM and AFM results, we find that the nanowire-like pattern observed on the HOPG surface was not seen on the mica surface. This could be due to the fact that the π-π interaction at the molecule-HOPG interface is absent on the mica surface, which is consistent with previous reports.[53,56,57] These results imply that the liquid-solid interface plays a crucial role in the hierarchical on-surface self-arrangement of large and more complex nanostructures.

Probably due to the giant molecular frameworks, numerous attempts at growing crystals of triakis tetrahedron $\mathbf{S^2}$ have been performed but are so far without success. However, the good solubility of the as-developed 3D molecular cage in polar solvents grants us the possibility to elucidate the fine structure in solution via SAXS methodology.[51] Accordingly, SAXS data were collected and depicted in Figure 5I. Typical scattering features of sphere-like nanoparticles can be observed from the experimental SAXS curves of $\mathbf{S^2}$. Bearing the precise coordinated structures of the assembled $\mathbf{S^2}$ in mind, theoretical scattering plot in solution is able to be accessible from the Crysol software packages. The experimental SAXS data are found to match well with the above-mentioned theoretical scattering plot suggesting from the first local minimum (Q = 0.13 $Å^{-1}$) as well as the oscillation peaks (Q_{max1} = 0.19 $Å^{-1}$, Q_{max2} = 0.33 $Å^{-1}$) at the high Q region, which unambiguously demonstrate the successful preparation of the sophisticated isohedral triakis tetrahedron suprastructures.

Catalytic performance

To confirm a plausible practical application of the triakis tetrahedron $\mathbf{S^2}$, it was tested as a nanoreactor with catalytic activity. Here, triakis tetrahedron $\mathbf{S^2}$ was employed for the oxidative degradation reaction of sulfur mustard (2-chloroethyl ethyl sulfide [CEES]). Multiple $[Ru(tpy)_2]^{2+}$ moieties and the 3D porous skeleton of triakis tetrahedron $\mathbf{S^2}$ enabled reasonable $^1O_2$ production and oxidative degradation ability of CEES (Figures S67–S69). This result provides a new construct for promising photocatalysts, and other catalytic reactions are expected to be explored. Given the unique architecture of the triakis tetrahedron, there is promise for further work exploring host-guest catalysis.

In summary, a novel tetrahedral architecture has been successfully built up through the efficient self-recognition of Ru-based MOL ligand with multi-topic tpy ligands in near-quantitative yield. A tetrahedral cage is capped by trigonal-pyramidal cages to generate a triakis tetrahedron. Planar Ru(II)-linked metal-organic ligands and non-planar hexafunctionalized tribenzotriquinacene cavitand-shaped ligands serve as scaffolds for the formation of the 3D triakis tetrahedron. The molecular composition and size analysis of triakis tetrahedron $\mathbf{S^2}$ were clearly determined using NMR, ESI-MS, ESI-TWIM-MS, TEM, STM, AFM, DLS, and SAXS experiments. The non-planar core that provides multi-topic bridges is crucial for the formation of the 3D triakis tetrahedron. This work points to the fact that the self-assembly of elaborate 3D triakis solids such as a triakis octahedron can be envisioned and achieved through delicate molecular designs. The heteroleptic and controllable self-assembly in this study enhances the topological diversity of known supramolecular coordination polyhedra.

EXPERIMENTAL PROCEDURES

Resource availability

Lead contact

Further information and requests for resources and reagents should be directed to and will be fulfilled by the lead contact, Pingshan Wang (chemwps@csu.edu.cn).

Materials availability

All unique reagents generated in this study are available from the lead contact without restriction.

Data and code availability

All of the data supporting the findings of this study are presented within the article and the supplemental experimental procedures. Any requests for additional data will be fulfilled by the lead contact upon reasonable request.

Self-assembly of triakis tetrahedron S^2

Ligand L^1 (3.48 mg, 1.36 μmol), ligand L^3 (3.41 mg, 0.90 μmol), and $Cd(NO_3)_2 \cdot 4H_2O$ (1.66 mg, 5.40 μmol) were added in a 50 mL flask, then a solvent mixture of CH_3CN/MeOH (20 mL, V:V, 2:1) was added. The mixture was refluxed for 12 h; after cooling to ambient temperature, excess $LiNTf_2$ in MeOH was added to get a red precipitate, which was filtered and washed with MeOH to generate a red solid: 10.5 mg, 97%. The characterization results are as follows: ^{1}H NMR (400 MHz, CD_3CN, ppm): δ8.99 (s, 48H, C-tpy-$H^{3',5'}$); δ8.73–8.69 (m, 72H, A-tpy-$H^{3',5'}$, C-tpy-$H^{3,3''}$); δ8.45 (s, 48H, B-tpy-$H^{3',5'}$); δ8.35–8.33 (m, 48H, B-tpy-$H^{3,3''}$); δ8.25–8.23 (m, 72H, A-tpy-$H^{3,3''}$, C-Ph-H^g); δ8.08–8.01 (m, 120H, B-tpy-$H^{4,4''}$, B-Ph-H^g, Ph-H^e); δ7.93–7.84 (m, 72H, C-tpy-$H^{4,4''}$, A-Ph-H^g); δ7.73–7.61 (m, 168H, A-tpy-$H^{4,4''}$, B-tpy-$H^{6,6''}$, B-Ph-H^h, C-Ph-H^h); δ7.42–7.35 (m, 72H, B-tpy-$H^{5,5''}$, C-tpy-$H^{5,5''}$); δ7.04–6.96 (m, 48H, A-tpy-$H^{6,6''}$, A-Ph-H^h); δ6.90–6.86 (m, 24H, A-tpy-$H^{5,5''}$); δ6.71–6.62 (m, 48H, Ph-H^i); δ5.77–5.72 (m, 96H, Ph-H^i); δ4.15 (s, 48H, OMe-H^b); δ3.95–3.93 (m, 96H, OMe-H^a); δ2.76–2.64 (m, 288H, OMe-H^f). ESI-MS (48,284.86 calculated for $C_{1964}H_{1380}Cd_{24}F_{360}N_{240}O_{372}Ru_6S_{120}$ with NTf_2^-): *m/z*: 2,401.96 $[M-18NTf_2]^{18+}$ (calculated *m/z*: 2,402.35); 2,261.06 $[M-19NTf_2]^{19+}$ (calculated *m/z*: 2,261.16); 2,133.95 $[M-20NTf_2]^{20+}$ (calculated *m/z*: 2,134.10); 2019.10 $[M-21NTf_2]^{21+}$ (calculated *m/z*: 2,019.13); 1,914.59 $[M-22NTf_2]^{22+}$ (calculated *m/z*: 1,914.62); 1,818.99 $[M-23NTf_2]^{23+}$ (calculated *m/z*: 1,819.20); 1,731.61 $[M-24NTf_2]^{24+}$ (calculated *m/z*: 1,731.42); 1,651.22 $[M-25NTf_2]^{25+}$ (calculated *m/z*: 1,651.25); 1,576.98 $[M-26NTf_2]^{26+}$ (calculated *m/z*: 1,576.96); 1,508.25 $[M-27NTf_2]^{27+}$ (calculated *m/z*: 1,508.18); 1,444.35 $[M-28NTf_2]^{28+}$ (calculated *m/z*: 1,444.31); 1,384.63 $[M-29NTf_2]^{29+}$ (calculated *m/z*: 1,384.85); 1,329.12 $[M-30NTf_2]^{30+}$ (calculated *m/z*: 1,329.35); 1,277.54$[M-31NTf_2]^{31+}$ (calculated *m/z*: 1,277.43); 1,228.67 $[M-32NTf_2]^{32+}$ (calculated *m/z*: 1,228.76); 1,182.69 $[M-33NTf_2]^{33+}$ (calculated *m/z*: 1,183.03); 1,139.83 $[M-34NTf_2]^{34+}$ (calculated *m/z*: 1,140.00); 1,099.39 $[M-35NTf_2]^{35+}$ (calculated *m/z*: 1,099.42); 1,061.02 $[M-36NTf_2]^{36+}$ (calculated *m/z*: 1,061.10); 1,024.76 $[M-37NTf_2]^{37+}$ (calculated *m/z*: 1,024.85). For additional information on characterization and experimental procedures, please see the supplemental experimental procedures.

SUPPLEMENTAL INFORMATION

Supplemental information can be found online at https://doi.org/10.1016/j.xcrp.2023.101293.

ACKNOWLEDGMENTS

We acknowledge the support from National Natural Science Foundation of China (21971257, 22101060, and 22101302) and Hunan Provincial Science and Technology Plan Project of China (no. 2019TP1001), the Guangdong Natural Science Foundation (2022A1515012187), and the Science and Technology Research Project of Guangzhou (202201020201 and 202102010432). KW. acknowledges the support from the US National Science Foundation (OIA-1757220).

AUTHOR CONTRIBUTIONS

Z.J. and P.W. conceived the project and designed the experiments. Z.J. and J.W. completed the synthesis. W.L., Z.W., B.C., and Z.J. analyzed the NMR experimental data. M.C. performed MS characterization. H.Z. and K.W. conducted STM and AFM characterization. J.-F.Y. and P.Y. conducted SAXS characterization. Y.L. and Y.-T.C. developed the manuscript. Z.J., J.W., H.Z., and M.C. analyzed the data and wrote the manuscript. P.W. and K.W. revised and supervised the manuscript. All the authors discussed the results and commented and proofread the manuscript.

DECLARATION OF INTERESTS

The authors declare no competing interests.

Received: October 20, 2022
Revised: December 29, 2022
Accepted: January 24, 2023
Published: February 16, 2023

REFERENCES

1. Alvarez, S. (2005). Polyhedra in (inorganic) chemistry. Dalton Trans. 2209–2233.
2. Edwardson, T.G.W., Levasseur, M.D., Tetter, S., Steinauer, A., Hori, M., and Hilvert, D. (2022). Protein cages: from fundamentals to advanced applications. Chem. Rev. *122*, 9145–9197.
3. Hogle, J.M., Chow, M., and Filman, D.J. (1985). Three-dimensional structure of poliovirus at 2.9 A resolution. Science *229*, 1358–1365.
4. Hsia, Y., Bale, J.B., Gonen, S., Shi, D., Sheffler, W., Fong, K.K., Nattermann, U., Xu, C., Huang, P.S., Ravichandran, R., et al. (2016). Design of a hyperstable 60-subunit protein icosahedron. Nature *535*, 136–139.
5. Li, Y., Tian, C., Liu, Z., Jiang, W., and Mao, C. (2015). Structural transformation: assembly of an otherwise inaccessible DNA nanocage. Angew. Chem. Int. Ed. Engl. *54*, 5990–5993.
6. Bale, J.B., Gonen, S., Liu, Y., Sheffler, W., Ellis, D., Thomas, C., Cascio, D., Yeates, T.O., Gonen, T., King, N.P., and Baker, D. (2016). Accurate design of megadalton-scale two-component icosahedral protein complexes. Science *353*, 389–394.
7. McTernan, C.T., Davies, J.A., and Nitschke, J.R. (2022). Beyond platonic: how to build metal–organic polyhedra capable of binding low-symmetry, information-rich molecular cargoes. Chem. Rev. *122*, 10393–10437.
8. Stang, P.J., and Olenyuk, B. (1997). Self-assembly, symmetry, and molecular architecture: coordination as the motif in the rational design of supramolecular metallacyclic polygons and polyhedra. Acc. Chem. Res. *30*, 502–518.
9. Lee, S., Jeong, H., Nam, D., Lah, M.S., and Choe, W. (2021). The rise of metal–organic polyhedra. Chem. Soc. Rev. *50*, 528–555.
10. Wu, T., Jiang, Z., Bai, Q., Li, Y., Mao, S., Yu, H., Wojtas, L., Tang, Z., Chen, M., Zhang, Z., et al. (2021). Supramolecular triangular orthobicupola: self-assembly of a giant Johnson solid J27. Chem *7*, 2429–2441.
11. Sudan, S., Li, R.-J., Jansze, S.M., Platzek, A., Rudolf, R., Clever, G.H., Fadaei-Tirani, F., Scopelliti, R., and Severin, K. (2021). Identification of a heteroleptic $Pd_6L_6L'_6$ coordination cage by screening of a virtual combinatorial library. J. Am. Chem. Soc. *143*, 1773–1778.
12. Davies, J.A., Ronson, T.K., and Nitschke, J.R. (2022). Twisted rectangular subunits self-assemble into a ferritin-like capsule. Chem *8*, 1099–1106.
13. Handke, M., Adachi, T., Hu, C., and Ward, M.D. (2017). Encapsulation of isolated luminophores within supramolecular cages. Angew. Chem. Int. Ed. Engl. *56*, 14003–14006.
14. Gemen, J., Białek, M.J., Kazes, M., Shimon, L.J.W., Feller, M., Semenov, S.N., Diskin-Posner, Y., Oron, D., and Klajn, R. (2022). Ternary host-guest complexes with rapid exchange kinetics and photoswitchable fluorescence. Chem *8*, 2362–2379.
15. Lu, Y.-L., Song, J.-Q., Qin, Y.-H., Guo, J., Huang, Y.-H., Zhang, X.-D., Pan, M., and Su, C.-Y. (2022). A redox-active supramolecular Fe_4L_6 cage based on organic vertices with acid–base-dependent charge tunability for dehydrogenation catalysis. J. Am. Chem. Soc. *144*, 8778–8788.
16. Tan, C., Jiao, J., Li, Z., Liu, Y., Han, X., and Cui, Y. (2018). Design and assembly of a chiral metallosalen-based octahedral coordination cage for supramolecular asymmetric catalysis. Angew. Chem. Int. Ed. Engl. *57*, 2085–2090.
17. Turunen, L., Warzok, U., Schalley, C.A., and Rissanen, K. (2017). Nano-sized $I_{12}L_6$ molecular capsules based on the [N•••I+•••N] halogen bond. Chem *3*, 861–869.
18. Clever, G.H., and Punt, P. (2017). Cation-anion arrangement patterns in self-assembled Pd_2L_4 and Pd_4L_8 coordination cages. Acc. Chem. Res. *50*, 2233–2243.
19. Zhang, D., Ronson, T.K., Lavendomme, R., and Nitschke, J.R. (2019). Selective separation of polyaromatic hydrocarbons by phase transfer of coordination cages. J. Am. Chem. Soc. *141*, 18949–18953.
20. Hou, Y.-J., Wu, K., Wei, Z.-W., Li, K., Lu, Y.-L., Zhu, C.-Y., Wang, J.-S., Pan, M., Jiang, J.-J., Li, G.-Q., and Su, C.-Y. (2018). Design and enantioresolution of homochiral Fe(II)–Pd(II) coordination cages from stereolabile metalloligands: stereochemical stability and enantioselective separation. J. Am. Chem. Soc. *140*, 18183–18191.
21. Shi, Y., Cai, K., Xiao, H., Liu, Z., Zhou, J., Shen, D., Qiu, Y., Guo, Q.-H., Stern, C., Wasielewski, M.R., et al. (2018). Selective extraction of C70 by a tetragonal prismatic porphyrin cage. J. Am. Chem. Soc. *140*, 13835–13842.
22. Nguyen, B.-N.T., Thoburn, J.D., Grommet, A.B., Howe, D.J., Ronson, T.K., Ryan, H.P., Bolliger, J.L., and Nitschke, J.R. (2021). Coordination cages selectively transport molecular cargoes across liquid membranes. J. Am. Chem. Soc. *143*, 12175–12180.
23. Bell, D.J., Natrajan, L.S., and Riddell, I.A. (2022). Design of lanthanide based metal–organic polyhedral cages for application in catalysis, sensing, separation and magnetism. Coord. Chem. Rev. *472*, 214786.
24. Percástegui, E.G., Ronson, T.K., and Nitschke, J.R. (2020). Design and applications of water-soluble coordination cages. Chem. Rev. *120*, 13480–13544.
25. Ahmad, N., Younus, H.A., Chughtai, A.H., and Verpoort, F. (2015). Metal–organic molecular cages: applications of biochemical implications. Chem. Soc. Rev. *44*, 9–25.
26. El-Sayed, E.-S.M., Yuan, Y.D., Zhao, D., and Yuan, D. (2022). Zirconium metal–organic cages: synthesis and applications. Acc. Chem. Res. *55*, 1546–1560.
27. Virovets, A.V., Peresypkina, E., and Scheer, M. (2021). Structural chemistry of giant metal based supramolecules. Chem. Rev. *121*, 14485–14554.

28. Pasquale, S., Sattin, S., Escudero-Adán, E.C., Martínez-Belmonte, M., and de Mendoza, J. (2012). Giant regular polyhedra from calixarene carboxylates and uranyl. Nat. Commun. *3*, 785.

29. Conn, M.M., and Rebek, J. (1997). Self-assembling capsules. Chem. Rev. *97*, 1647–1668.

30. Liu, D., Li, K., Chen, M., Zhang, T., Li, Z., Yin, J.-F., He, L., Wang, J., Yin, P., Chan, Y.-T., and Wang, P. (2021). Russian-Doll-Like molecular cubes. J. Am. Chem. Soc. *143*, 2537–2544.

31. Ubasart, E., Borodin, O., Fuertes-Espinosa, C., Xu, Y., García-Simón, C., Gómez, L., Juanhuix, J., Gándara, F., Imaz, I., Maspoch, D., et al. (2021). A three-shell supramolecular complex enables the symmetry-mismatched chemo- and regioselective bis-functionalization of C_{60}. Nat. Chem. *13*, 420–427.

32. Tominaga, M., Suzuki, K., Kawano, M., Kusukawa, T., Ozeki, T., Sakamoto, S., Yamaguchi, K., and Fujita, M. (2004). Finite, spherical coordination networks that self-organize from 36 small components. Angew. Chem. Int. Ed. Engl. *43*, 5621–5625.

33. Sun, Q.-F., Iwasa, J., Ogawa, D., Ishido, Y., Sato, S., Ozeki, T., Sei, Y., Yamaguchi, K., and Fujita, M. (2010). Self-assembled $M_{24}L_{48}$ polyhedra and their sharp structural switch upon subtle ligand variation. Science *328*, 1144–1147.

34. Fujita, D., Ueda, Y., Sato, S., Yokoyama, H., Mizuno, N., Kumasaka, T., and Fujita, M. (2016). Self-assembly of $M_{30}L_{60}$ icosidodecahedron. Chem *1*, 91–101.

35. Fujita, D., Ueda, Y., Sato, S., Mizuno, N., Kumasaka, T., and Fujita, M. (2016). Self-assembly of tetravalent Goldberg polyhedra from 144 small components. Nature *540*, 563–566.

36. Gosselin, A.J., Rowland, C.A., and Bloch, E.D. (2020). Permanently microporous metal-organic polyhedra. Chem. Rev. *120*, 8987–9014.

37. Cao, L., Wang, P., Miao, X., Dong, Y., Wang, H., Duan, H., Yu, Y., Li, X., and Stang, P.J. (2018). Diamondoid supramolecular coordination frameworks from discrete adamantanoid platinum(II) cages. J. Am. Chem. Soc. *140*, 7005–7011.

38. Morimoto, M., Bierschenk, S.M., Xia, K.T., Bergman, R.G., Raymond, K.N., and Toste, F.D. (2020). Advances in supramolecular host-mediated reactivity. Nat. Catal. *3*, 969–984.

39. Koo, J., Kim, I., Kim, Y., Cho, D., Hwang, I.-C., Mukhopadhyay, R.D., Song, H., Ko, Y.H., Dhamija, A., Lee, H., et al. (2020). Gigantic porphyrinic cages. Chem *6*, 3374–3384.

40. Zhou, X.-P., Wu, Y., and Li, D. (2013). Polyhedral metal-imidazolate cages: control of self-assembly and cage to cage transformation. J. Am. Chem. Soc. *135*, 16062–16065.

41. Lin, J., Li, N., Yang, S., Jia, M., Liu, J., Li, X.-M., An, L., Tian, Q., Dong, L.-Z., and Lan, Y.-Q. (2020). Self-assembly of giant Mo_{240} hollow opening dodecahedra. J. Am. Chem. Soc. *142*, 13982–13988.

42. Domoto, Y., Abe, M., and Fujita, M. (2021). A highly entangled $(M_3L_2)_8$ truncated cube from the anion-controlled oligomerization of a π-coordinated M_3L_2 subunit. J. Am. Chem. Soc. *143*, 8578–8582.

43. Chen, Y.-S., Solel, E., Huang, Y.-F., Wang, C.-L., Tu, T.-H., Keinan, E., and Chan, Y.-T. (2019). Chemical mimicry of viral capsid self-assembly via corannulene-based pentatopic tectons. Nat. Commun. *10*, 3443.

44. Wang, Z., He, L., Liu, B., Zhou, L.-P., Cai, L.-X., Hu, S.-J., Li, X.-Z., Li, Z., Chen, T., Li, X., and Sun, Q.-F. (2020). Coordination-assembled water-soluble anionic lanthanide organic polyhedra for luminescent labeling and magnetic resonance imaging. J. Am. Chem. Soc. *142*, 16409–16419.

45. Saha, R., Mondal, B., and Mukherjee, P.S. (2022). Molecular cavity for catalysis and formation of metal nanoparticles for use in catalysis. Chem. Rev. *122*, 12244–12307.

46. Zhao, X., Wang, H., Li, B., Zhang, W., Li, X., Zhao, W., Janiak, C., Heard, A.W., Yang, X.-J., and Wu, B. (2022). A hydrogen-bonded ravel assembled by anion coordination. Angew. Chem. Int. Ed. Engl. *61*, e202115042.

47. Zhu, F.-F., Chen, L.-J., Chen, S., Wu, G.-Y., Jiang, W.-L., Shen, J.-C., Qin, Y., Xu, L., and Yang, H.-B. (2020). Confinement self-assembly of metal-organic cages within mesoporous carbon for one-pot sequential reactions. Chem *6*, 2395–2406.

48. Scott, A.J., Vallejo, J., Sarkar, A., Smythe, L., Regincós Martí, E., Nichol, G.S., Klooster, W.T., Coles, S.J., Murrie, M., Rajaraman, G., et al. (2021). Exploiting host–guest chemistry to manipulate magnetic interactions in metallosupramolecular M_4L_6 tetrahedral cages. Chem. Sci. *12*, 5134–5142.

49. Hasui;, M., and Iwasaki, K. Triakis solids and harmonic functions.Preprint at arXiv, 10.48550/arXiv.1210.46811210.4681.

50. Weisstein, E.W. ("Triakis Tetrahedron." From MathWorld–A Wolfram Web Resource).

51. He, L., Hsu, H.-K., Li, L., Lin, L.-T., Tu, T.-H., Ong, T.-G., Liou, G.-G., and Chan, Y.-T. (2022). A 10-nm-sized multicompartment cuboctahedron and its 2D hierarchical arrays observed by cryo-EM. Chem *8*, 494–507.

52. He, L., Wang, S.-C., Lin, L.-T., Cai, J.-Y., Li, L., Tu, T.-H., and Chan, Y.-T. (2020). Multicomponent metallo-supramolecular nanocapsules assembled from calix[4] resorcinarene-based terpyridine ligands. J. Am. Chem. Soc. *142*, 7134–7144.

53. Adisoejoso, J., Tahara, K., Okuhata, S., Lei, S., Tobe, Y., and De Feyter, S. (2009). Two-dimensional crystal engineering: a four-component architecture at a liquid–solid interface. Angew. Chem. Int. Ed. Engl. *48*, 7353–7357.

54. Wang, H., Wang, K., Xu, Y., Wang, W., Chen, S., Hart, M., Wojtas, L., Zhou, L.-P., Gan, L., Yan, X., et al. (2021). Hierarchical self-assembly of nanowires on the surface by metallo-supramolecular truncated cuboctahedra. J. Am. Chem. Soc. *143*, 5826–5835.

55. Goll, F.D., Taubmann, G., and Ziener, U. (2022). Static scanning tunneling microscopy images reveal the mechanism of supramolecular polymerization of an oligopyridine on graphite. Angew. Chem. Int. Ed. Engl. *61*, e202117580.

56. Wang, H., Zhou, L.-P., Zheng, Y., Wang, K., Song, B., Yan, X., Wojtas, L., Wang, X.-Q., Jiang, X., Wang, M., et al. (2021). Double-layered supramolecular prisms self-assembled by geometrically non-equivalent tetratopic subunits. Angew. Chem. Int. Ed. Engl. *60*, 1298–1305.

57. Wang, M., Wang, K., Wang, C., Huang, M., Hao, X.-Q., Shen, M.-Z., Shi, G.-Q., Zhang, Z., Song, B., Cisneros, A., et al. (2016). Self-assembly of concentric hexagons and hierarchical self-assembly of supramolecular metal–organic nanoribbons at the solid/liquid interface. J. Am. Chem. Soc. *138*, 9258–9268.